PNAS RESEARCH ARTICLE | PHYSICS

Amplification mechanism with interacting atomic gases

Min Jiang[a,b,c,1], Yushu Qin[a,b,c,1], Yuanhong Wang[a,b,c], Ying Huang[a,b,c], Xinhua Peng[a,b,c,2], and Dmitry Budker[d,e,f,g]

Affiliations are included on p. 6.

Edited by Jonathan Breeze, University College London, London, United Kingdom; received September 25, 2024; accepted March 25, 2025 by Editorial Board Member Bernard F. Schutz

The use of atoms, molecules, and free electrons in quantum amplifiers has greatly advanced precision measurements, paving the way for the development of extremely-low-noise quantum devices such as masers and lasers. Here, we investigate the signal amplification of interacting spins and observe the amplification of magnetic fields using mixtures of interacting alkali-metal and noble gases. In contrast to noninteracting systems used as amplifiers, we demonstrate that interactions resulting from random atomic collisions give rise to two distinct amplification phenomena. These phenomena provide essential resources for enhancing quantum sensing capabilities. Our results show that magnetic fields can be amplified by at least two orders of magnitude, enhancing magnetic sensitivity to the femtotesla per root hertz level. Additionally, we report a counterpart phenomenon, deamplification, where the magnetic noise response is suppressed by at least one order of magnitude within certain frequency regimes. In this work alkali-metal and noble-gas spins are weakly coupled. We further explore how the performance of amplification changes with the interaction strength as the two spin gases gradually enter the strong-coupling regime, unveiling hitherto unexplored amplification effects that hold promise for enhancing precision measurements.

quantum amplification | interacting spins | noble gas | alkali metal

Significance

The use of physical systems as amplifiers has driven significant progress in precision measurements and offer a promising path to achieving precision beyond the standard limits. The key task now is to identify superior physical systems capable of realizing better quantum amplification. We report the magnetic amplification with interacting alkali-metal and noble-gas spins. Our work demonstrates that the alkali-noble interaction results in two distinct effects: magnetic amplification by over 100 and deamplification by over 10. These effects allow us to significantly enhance magnetic fields or suppress magnetic noise. We further investigate the amplification effect from the weak to strong interaction regimes and explore the potential for greater amplification. This work opens up exciting opportunities in the field of precision measurements.

Precision measurements of electromagnetic fields hold key importance in modern science and technology. Remarkable advances have been witnessed in the amplification of electromagnetic fields through the use of physical systems such as atoms, molecules, and free electrons as signal amplifiers (1–6). These groundbreaking achievements have enabled the amplification of electromagnetic fields with unprecedentedly low noise, facilitating diverse applications (4–10), such as deep-space communication receivers, radar systems, medical imaging, atomic clocks, and tests of fundamental symmetries. Various amplification technologies based on physical systems have driven the forefront of quantum electronics. For example, masers amplify microwaves in the frequency range of 10^8 to 10^{11} Hz (7–10). Similarly, lasers, which operate at higher frequencies, are crucial for applications in the visible light range of 10^{14} to 10^{15} Hz (6, 11). Recently, free-electron lasers have extended measurement capabilities to ultraviolet and X-rays, covering frequencies up to 10^{16} to 10^{17} Hz (4). Despite these significant achievements, the discovery of additional amplification systems remains a long-term research goal. This endeavor aims to advance in at least two key areas: improving amplifier performance-such as enhancing gain, widening bandwidth, and optimizing other critical metrics-and expanding the measurement frequency range of electromagnetic fields, including extremely low frequencies.

In this study, we investigate signal amplification with interacting atomic gases and demonstrate the amplification of magnetic fields using mixtures of interacting alkali-metal and noble-gas spin gases. The alkali metal is optically accessible, while the noble gas is long-lived but lacks optical transitions from the ground state. These atoms frequently engage in spin-exchange collision interactions with each other (12). Our study aims to address two key questions: 1) How do atomic interactions affect the electromagnetic response of spin gases? 2) What physical parameters of interacting systems are linked to signal amplification? By employing a spin mixture comprising alkali metals and noble gases undergoing random collision-induced interactions, we reveal that these interactions critically determine the magnetic field response, resulting in two distinct effects: amplification and deamplification. In the amplification regime, our experiments show that magnetic-field amplification can exceed two orders of magnitude. Consequently, we design an atomic amplifier with a remarkable sensitivity of 3.5 fT/Hz$^{1/2}$ at low frequencies below 100 Hz. Additionally, we present a counterpart device, the deamplifier, which is capable of suppressing magnetic noise by more than

Author contributions: M.J., X.P., and D.B. designed research; M.J., Y.Q., Y.H., X.P., and D.B. performed research; M.J., Y.Q., Y.W., Y.H., and X.P. contributed new reagents/analytic tools; M.J., Y.Q., Y.W., X.P., and D.B. analyzed data; and M.J., Y.Q., X.P., and D.B. wrote the paper.

The authors declare no competing interest.

This article is a PNAS Direct Submission. J.B. is a guest editor invited by the Editorial Board.

[1]M.J. and Y.Q. contributed equally to this work.

[2]To whom correspondence may be addressed. Email: xhpeng@ustc.edu.cn.

This article contains supporting information online at https://www.pnas.org/lookup/suppl/doi:10.1073/pnas.2419683122/-/DCSupplemental.

Published May 8, 2025.

10 times within certain frequency regimes. We further explore the amplification effects when alkali-metal and noble-gas spins enter a strongly interacting regime, uncovering previously unexplored amplification phenomena that hold promise as valuable resources for metrology. Our findings present exciting opportunities in the realm of precision measurements ranging from geophysics exploration to dark matter searches (13–17).

Results and Discussion

The experiments are carried out in a vapor cell that contains ^{87}Rb and ^{129}Xe gases-one that is optically accessible and another that is long-lived (Fig. 1*A*) (*SI Appendix, Experimental setup*). These two atomic gases interact with each other through Fermi-contact spin-exchange collisions (12). Although the collisions are random, they can be divided into incoherent and coherent collision processes (18, 19). The optically inaccessible ^{129}Xe spins are polarized along z through incoherent collisions with optically polarized ^{87}Rb atoms (12, 20). The coherent part of the random collisions leads to an interaction between the two spins, where alkali-metal spins experience an additional effective magnetic field $\lambda\mathbf{M}^b(t)$ and noble-gas nuclear spins experience $\lambda\mathbf{M}^a(t)$ as well. Here, $\lambda = 8\pi\kappa_0/3$ and $\kappa_0 \approx 540$ is the Fermi-contact enhancement factor for ^{87}Rb and ^{129}Xe (12, 20). To make the coherent dynamics of the two spin gases more intuitive, we use the Holstein-Primakoff transformation, i.e., $\hat{a} = (M_x^a + iM_y^a)/\sqrt{2\gamma_a M_z^a}$ and $\hat{b} = (M_x^b + iM_y^b)/\sqrt{2\gamma_b M_z^b}$ (21). The external measured field is assumed to be so weak that the excited transverse field M_x^a and M_y^a satisfy $M_x^a, M_y^a \ll M_z^a$. In the interacting atomic gases, we show that the spin excitations $\hat{a}$ and $\hat{b}$ are coupled with each other and their dynamics can be modeled by ref. 18, *SI Appendix, Interacting spin gases*

$$\partial_t \begin{pmatrix} \hat{a} \\ \hat{b} \end{pmatrix} = i \begin{pmatrix} \omega_a + i\Gamma_a & -J \\ -J & \omega_b + i\Gamma_b \end{pmatrix} \begin{pmatrix} \hat{a} \\ \hat{b} \end{pmatrix} + \begin{pmatrix} h_a \\ h_b \end{pmatrix}, \qquad [1]$$

where $\omega_a = \gamma_a(B_z + \lambda M_z^b)$ and $\omega_b = \gamma_b(B_z + \lambda M_z^a)$ denotes the Larmor frequency of the alkali-metal spin and noble-gas spin, respectively. Here, $\gamma_{a,b}$ are gyromagnetic ratios and $\Gamma_{a,b}$ are decoherence rates. Importantly, the excitations $\hat{a}$ and $\hat{b}$ have a bidirectional interaction described with $J = \lambda\sqrt{\gamma_a\gamma_b M_z^a M_z^b}$ (18). In our experiment, the ^{87}Rb to ^{129}Xe bidirectional interaction is measured to be approximately $J/2\pi \approx 4.8$ Hz. With the optimizations discussed below, this interaction J can potentially be increased to over 100 Hz. The last term with $h_{a,b}$ represents the excitations induced by the measured field (*SI Appendix, Interacting spin gases*), such as normal magnetic field and pseudomagnetic field from inertial rotation or hypothetical particles beyond the standard model. The signal response of interacting atomic gases is acquired by measuring the excitation of alkali metals $\hat{a}$ through optical probing of the alkali metal (Fig. 1*A*) (22, 23).

Bidirectional interaction between two spin gases produces an interference between alkali-metal and noble-gas spin responses. This is depicted in Fig. 1 *B* and *C*, ^{87}Rb spins exhibit a broad magnetic resonance line ($\Gamma_a/2\pi \approx 1.6$ kHz), while ^{129}Xe nuclear spins possess a narrower resonance line ($\Gamma_b/2\pi \approx 1.2$ mHz). As a consequence of their distinct resonance lines, the ^{129}Xe response phase exhibits a π jump at its resonance and, by contrast, the ^{87}Rb response phase varies slowly. When compared to the response of pure alkali-metal spins, regarded as the magnitude of the calibrated magnetic field signal, the interference between ^{87}Rb and ^{129}Xe spin excitations arises due to the coupling between these spins and further results in an asymmetric response profile of ^{87}Rb near the ^{129}Xe resonance frequency (Fig. 1*D*).

We show that the power spectrum of the asymmetric signal response can be well described as a Fano profile (*SI Appendix, Fano resonance*)

$$F(\epsilon) = \mathscr{A}(\epsilon)\frac{(q+\epsilon)^2}{1+\epsilon^2} + \mathscr{B}(\epsilon), \qquad [2]$$

where $\epsilon = (\omega - \widetilde{\omega}_b)/\widetilde{\Gamma}_b = 2\pi(\nu - \widetilde{\nu}_b)/\widetilde{\Gamma}_b$, $\widetilde{\omega}_b$ and $\widetilde{\Gamma}_b$ is the dressed ^{129}Xe Larmor frequency and the rate of decoherence due to the bidirectional ^{87}Rb to ^{129}Xe interaction (see *Discussion* below). Here, q denotes the Fano parameter, which affects the symmetry of the profile. The first term in Eq. **2** is asymmetric when the Fano parameter q is nonzero, where the profile shape reverses when the sign of q changes. When q is close to zero, the profile becomes symmetric. The factor $\mathscr{A}(\epsilon)$ is the individual ^{87}Rb response to the oscillating field, characterized by a symmetric profile (*SI Appendix, Fano resonance*) and the factor $(q+\epsilon)^2/(1+\epsilon^2)$ only depends on noble gas. It is noteworthy

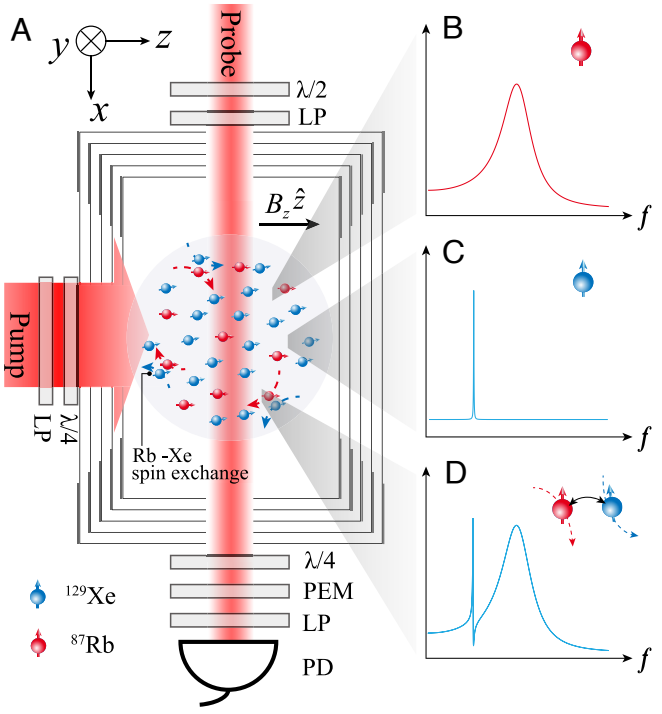

Fig. 1. Principle of signal amplification using interacting atomic spin gases. (*A*) Experimental setup. The key element is a 0.5 cm^3 vapor cell containing 20 torr ^{129}Xe, 250 torr N_2, and a droplet of isotopically enriched ^{87}Rb. ^{129}Xe spins are polarized and coupled with ^{87}Rb by Fermi-contact collisions. ^{87}Rb atoms are polarized with a circularly polarized pump laser light tuned to the D1 line and probed with a linearly polarized probe laser light detuned to higher frequencies by about 100 GHz from the D2 line. PEM, photoelastic modulator; $\lambda/4$, quarter-wave Plate; PD, photodiode; and LP, linear polarizer. (*B* and *C*) Magnetic responses of individual alkali metals and noble gases, respectively. The individual Rb system provides a symmetric response profile with a broad resonance linewidth $\Gamma_a/2\pi \approx 1.6$ kHz (red line), while the ^{129}Xe response profile features a narrower linewidth of $\Gamma_b/2\pi \approx 1.2$ mHz (blue line). (*D*) Response altered by the interactions. The coupled alkali–noble-gas spins can be seen as two coupled harmonic oscillators. In the interacting ^{87}Rb to ^{129}Xe system, apart from the symmetric response component, there is also an asymmetric Fano profile near the ^{129}Xe resonance frequency. In the vicinity of the ^{129}Xe resonance frequency, a notable response amplification and deamplification phenomena occur as a result of interaction-induced interference.

that the first part of the total response $F(\epsilon)$ can be described as a product of these two factors, which quantitatively characterizes the interference between interacting alkali-metal and noble-gas spins. The factor $\mathscr{B}(\epsilon)$ is the noninterference term, which depends on both alkali metal and noble gas. $\mathscr{B}(\epsilon)$ is relatively symmetric compared to the factor $(q+\epsilon)^2/(1+\epsilon^2)$. As the background of the profile, its amplitude relative to the first term significantly affects the symmetry characteristics of the profile (*SI Appendix, Fano resonance*). Consequently, two distinct amplification phenomena emerge. Constructive interference at $\epsilon = 0$, which corresponds to signal enhancement that reaches a maximum amplitude of $\approx|q|\mathscr{A}^{1/2}(\epsilon)$. We find the amplification factor of the signal amplitude is $|q|$. Destructive interference at $\epsilon = -q$, which corresponds to signal suppression. These phenomena are referred to as "amplification" and "deamplification," respectively.

In our experiments, we verify the aforementioned asymmetric Fano resonance and the corresponding amplification/deamplification phenomena. As an example, the external magnetic field is set as $B_z \approx -8.59$ mG, corresponding to $\omega_b/2\pi \approx 10.11$ Hz. We apply an oscillating test field along y and sweep its oscillation frequency around ω_b, and record the frequency-response signal. The measurement duration of each point in our experiment is 180 s. Fig. 2*A* shows the experimental data, where each curve exhibits an asymmetric profile. Here, the response of individual ^{87}Rb atoms is flat near the ^{129}Xe resonance frequency and can therefore be taken as the normalization amplitude. Taking the dark-blue line as an example, when the oscillation frequency ν is near $\widetilde{\nu}_b \approx 10.11$ Hz (corresponding to $\epsilon \approx 0$), the magnetic-field response amplitude [i.e., the square root of the power $F(\epsilon)$] is greatly enhanced by a factor of $|q| \approx 524$. While at about 8.05 Hz (corresponding to $\epsilon \approx -q$), the magnetic-field response is suppressed by at least one order of magnitude.

The Fano parameter q reflects the magnitude of the interaction between the discrete state ^{129}Xe and the continuous state Rb in the interacting gases. Since our system reads out the ^{87}Rb spins optically, the Fano parameter indicates the enhancement effect of ^{129}Xe on the ^{87}Rb response, particularly the amplification at the resonance frequency. The Fano parameter q can be derived as (*SI Appendix, Signal amplification*),

$$q \approx \frac{\gamma_b \lambda M_z^b}{2\widetilde{\Gamma}_b}, \qquad [3]$$

and its absolute value $|q|$ represents the amplification factor. This amplification relies on two factors: the decoherence rate $\widetilde{\Gamma}_b$ of ^{129}Xe, which is six orders of magnitude smaller than Rb, and the magnitude of the effective field exerted by ^{129}Xe on ^{87}Rb. This effective field is proportional to the number density and polarization of the noble gas, given a specific Fermi contact enhancement factor for the spins. Furthermore, we can also change the effective field at the ^{129}Xe resonant frequency by applying a z-direction AC field $B_{ac}\cos\omega_{ac}t$. The effective field is modulated as $\lambda M_z^{b'} = \lambda M_z^b \mathscr{J}_0^2(\gamma_b B_{ac}/\omega_{ac})$, where $\mathscr{J}_0$ is the Bessel function of the first kind of order zero (*SI Appendix, Fano parameter modification*). Fig. 2*B* provides a magnified view of the amplification regime in Fig. 2*A*, illustrating the amplification behavior for different values of $q \approx \gamma_b \lambda M_z^{b'}/2\widetilde{\Gamma}_b$.

As a counterpart to amplification, deamplification with a minimum response occurs at $\epsilon \approx -q$, according to Eq. **2**. Fig. 2*C* shows that the frequency of maximum deamplification shifts $\Delta\nu$ from the ^{129}Xe resonance linearly with the Fano parameter q, i.e., $\Delta\nu = \nu - \widetilde{\nu}_b \approx q \cdot 0.004$ Hz. A theoretical derivation gives $\Delta\nu \approx q\widetilde{\Gamma}_b/2\pi$ (*SI Appendix, Signal amplification*). Consequently, the fit to the data gives $\widetilde{\Gamma}_b \approx [40\text{ s}]^{-1}$, which is in good agreement with independent measurements of the ^{129}Xe spin-decoherence rate. As discussed below, although the magnetic responsivity deteriorates in the deamplification regime, this approach is well suited for suppressing environmental magnetic noise by at least one order of magnitude.

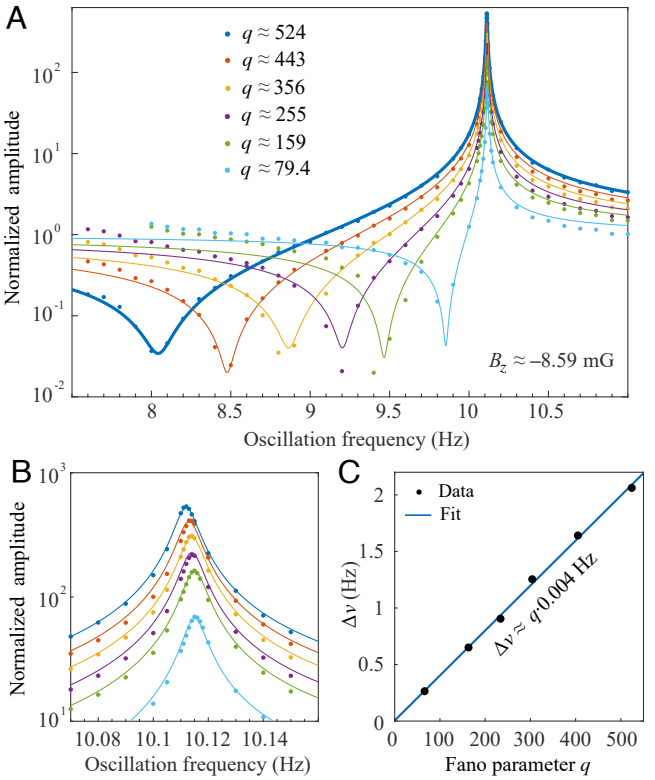

Fig. 2. Demonstration of signal amplification and deamplification. (*A*) Response profile as a function of the frequency of y-directed measured field. B_z is set to about −8.59 mG as an example. The response at 80 Hz is taken as the normalization amplitude. The data are well fit with theoretical Fano profile with Fano parameter q, which is modified by applying a periodic magnetic field (*SI Appendix, Fano parameter modification*). For each profile, there exists an amplification regime with large response above one and a deamplification regime with response below one. (*B*) Amplification with varying Fano parameters q (Partial enlarged view of Fig. 2*A*). (*C*) Deamplification with respect to Fano parameter. The deamplification frequency is linearly dependent on the Fano parameter with the slope of 0.004 (see text).

The amplification and deamplification depend on the noble-gas decoherence rate $\widetilde{\Gamma}_b$. We show below that the bidirectional interaction and the external magnetic field can modify this rate. By diagonalizing the matrix in Eq. **1**, we obtain the dressed Larmor frequencies $\widetilde{\omega}_{a,b}$ and decoherence rates $\widetilde{\Gamma}_{a,b}$ of the interacting spins (*SI Appendix, Interacting spin gases*):

$$\widetilde{\omega}_{a,b} + i\widetilde{\Gamma}_{a,b} = \omega_0 + i\chi \pm \sqrt{J^2 + \Gamma^2}, \qquad [4]$$

where $\omega_0 = (\omega_a + \omega_b)/2$, $\chi = (\Gamma_a + \Gamma_b)/2$ and $\Gamma = \delta + i\beta$ with $\delta = (\omega_a - \omega_b)/2$, $\beta = (\Gamma_a - \Gamma_b)/2$. We show that the joint action of the magnetic Zeeman interaction and the alkali–noble-gas bidirectional interaction dresses their Larmor frequencies and decoherence rates. In the following, we focus on the decoherence rate $\widetilde{\Gamma}_b$ of ^{129}Xe spins. According to Eq. **4**, the noble-gas decoherence rate is $\widetilde{\Gamma}_b = \chi - \mathbf{Im}\left[J^2 + (\delta + i\beta)^2\right]^{1/2}$. As shown

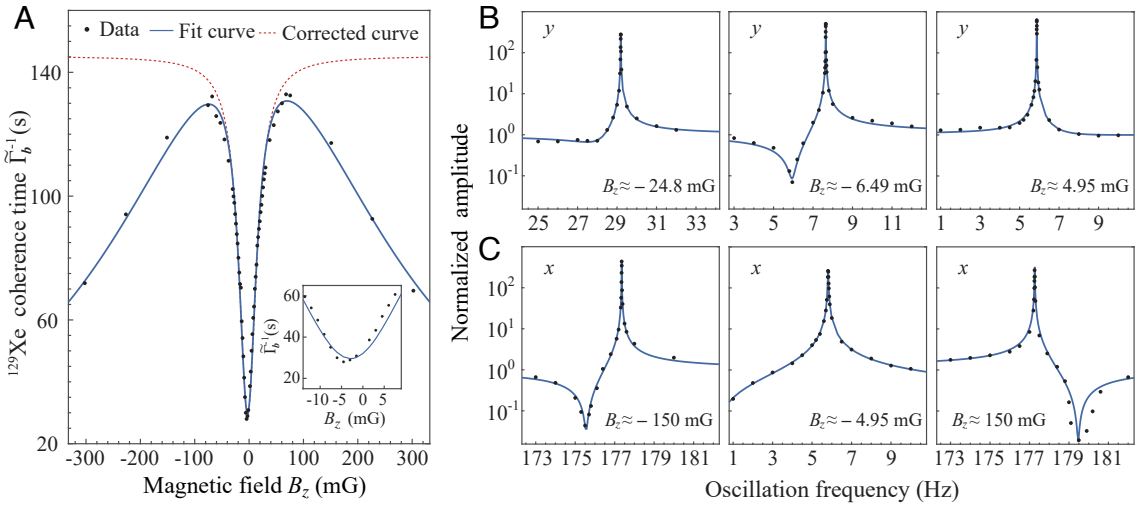

Fig. 3. Signal response modified with an external magnetic field. (*A*) ^{129}Xe coherence time as a function of external magnetic field. The ^{129}Xe decoherence rate reaches a maximum $\tilde{\Gamma}_b \approx [28\,\mathrm{s}]^{-1}$ at $B_z \approx -3$ mG and reaches a minimum $\tilde{\Gamma}_b \approx [130\,\mathrm{s}]^{-1}$ at $B_z \approx \pm 70$ mG. After increasing external field, the coherence time decreases due to magnetic field gradient. The solid line is the theoretical fit with our built noble-gas decoherence model. Based on our analysis (*SI Appendix, Noble-gas spin decoherence model*), the magnetic field inhomogeneity is estimated to be about 0.04%. The dashed line represents the ^{129}Xe decoherence after numerically correcting the magnetic field gradient. (*B* and *C*) Response profiles for *x*, *y*-direction oscillating fields under different bias fields.

in the Appendix, the maximum of $\tilde{\Gamma}_b$ can be theoretically given by calculating the extreme value of $\tilde{\Gamma}_b$. In our ^{87}Rb to ^{129}Xe experiment, we observe that J/β satisfies $J/\beta \approx 6 \times 10^{-3} \ll 1$, indicating that the alkali–noble-gas interaction strength is significantly smaller than the alkali-metal decoherence rate. This is commonly referred to as the weak coupling regime. In this regime, $\tilde{\Gamma}_b$ reaches a maximum $\tilde{\Gamma}_b \approx \Gamma_b + J^2/2\beta$ at $\delta = 0$, where the electron and nuclear spin precession frequencies are nearly matched. Here, $\delta = 0$ corresponds to the external field $B_z = \lambda(\gamma_b M_z^a - \gamma_a M_z^b)/(\gamma_a - \gamma_b) \approx -\lambda M_z^b$. As shown in Fig. 3*A*, the experimental decoherence rate reaches a maximum $\tilde{\Gamma}_b \approx [28\,\mathrm{s}]^{-1}$ when the external applied field is $B_z \approx -3$ mG. These observations agree well with our theoretical analysis.

The ^{129}Xe decoherence rate decreases rapidly as B_z deviates from $-\lambda M_z^b$. At a bias field of $B_z \approx \pm 70$ mG, the decoherence rate reaches a minimum $\tilde{\Gamma}_b \approx [130\,\mathrm{s}]^{-1}$. This increase in coherence time (the reciprocal of $\tilde{\Gamma}_b$) from 28 s to 130 s is an important effect that should not be overlooked, even in the weak coupling regime. This observation underscores the importance of carefully setting the external magnetic field strength in precision measurement experiments that aim for extended noble-gas coherence times, such as comagnetometers (24, 25) and nuclear gyroscopes (26). Specifically, it is essential to decouple the two spin gases by deviating from $B_z \approx -\lambda M_z^b$. Further increases in B_z lead to a decrease in the ^{129}Xe coherence time due to the inhomogeneity of the B_z field. We numerically correct the gradient effects and obtain the decoherence rate $\tilde{\Gamma}_b$ (*SI Appendix, Noble-gas spin decoherence model*), represented by the dashed curve in Fig. 3*A*. We note that the decoherence rate could be restored to that of uncoupled ^{129}Xe spins, i.e., $\tilde{\Gamma}_b \approx \Gamma_b$ at the bias field larger than about 70 mG.

The deamplification depends on the external magnetic field. As shown in Fig. 3*B*, the response profile for the measured field along *y* gradually becomes symmetric as B_z increases. The reason for this phenomenon is that the influence of the noninterference term $\mathscr{B}(\epsilon)$ in the Fano formula cannot be ignored. As a symmetric background, it conceals the asymmetric features of the Fano resonance profile. In contrast, using the same method described above, we observe significant deamplification when an *x*-direction oscillating field is applied at large B_z, for example, $B_z \approx \pm 150$ mG in our experiment (Fig. 3*C*). The magnetic responsivity is enhanced by a factor over 200 in the amplification regime and suppressed by a factor over 10 in the deamplification regime. It is worth noting that the Fano profile (for example, with $B_z \approx \pm 150$ mG) is reversed in Fig. 3*C* due to the sign change of the Fano parameter q depending on the direction of the bias field. A theoretical explanation of the aforementioned phenomena is provided in the Appendix.

Summary and Outlook

The amplifier we developed, which can amplify magnetic fields below 100 Hz with exceptionally low noise, serves as a highly sensitive magnetometer. As shown in Fig. 4*A*, the magnetic sensitivity is improved to approximately 3.5 fT/Hz$^{1/2}$ at the ^{129}Xe Larmor frequency. This represents an improvement of more than two orders of magnitude over the photon-shot noise of the Rb probe laser. This technique opens up several intriguing applications. For example, the amplifier can serve as an ideal receiver for deep-sea communications. At hertz frequencies, electromagnetic fields exhibit strong diffraction and penetration capabilities, ensuring signal integrity over long distances (27). Using ^{129}Xe amplifiers as receivers may extend subsea communication ranges to tens or even hundreds of meters below sea level. Our work can also be applied to measure Schumann waves (13, 28), which are characterized by an oscillation frequency of approximately 7.83 Hz and its harmonics, originating from the resonance between the Earth's surface and the ionosphere. Unlike previous Schumann-resonance detectors such as SQUID magnetometers (28, 29), our approach could provide more sensitive sensors for capturing higher-order harmonics, thereby enriching our understanding of the Earth and its surrounding atmospheric conditions.

Our work introduces a quantum-sensing technique for measuring pseudomagnetic fields. A significant application of this technique is in the search for hypothetical particles beyond the standard model (30–32) such as ultralight axions or dark photons,

which are also well-motivated dark matter candidates. These particles can couple with standard-model particles (for example, to nuclei interacting with their spins) (33, 34) or act as force mediators to induce exotic interactions between two standard-model particles (16, 35). As a result, these particles generate an oscillating pseudomagnetic field on the spins. Here, the hypothetical particles are assumed to couple with only one of the alkali-metal and noble-gas spins. The amplifier presented in this work can in effect convert the pseudomagnetic field into an effective magnetic field that can be measured (*SI Appendix, Normal and pseudomagnetic response*). For example, the pseudomagnetic field on noble-gas spins can be effectively magnified by almost three orders of magnitude, achieving a sensitivity of 3.5 fT/Hz$^{1/2}$ (Fig. 4*B*). With our current experimental parameters, the sensitivity in searching for axions and dark photons could surpass the most stringent astrophysical constraints obtained from the supernova SN1987A cooling (36, 37). On the other hand, when magnetic noise is the dominant factor, it is preferable to choose the deamplification operation rather than amplification. In this scenario, the system's response to the pseudomagnetic field does not undergo destructive interference and its sensitivity is equal to the alkali-metal sensitivity (*SI Appendix, Normal and pseudomagnetic response*). In our experiment, this sensitivity is about 1 pT/Hz$^{1/2}$ with ^{87}Rb to ^{129}Xe system (Fig. 4*A*). However, using the K-^{3}He system may further improve this sensitivity, as the K magnetometer has already demonstrated sub-fT/Hz$^{1/2}$-level sensitivity, typically limited by magnetic noise from magnetic shields (22, 23). Consequently, deamplification can potentially overcome the magnetic noise limit, achieving sub-fT/Hz$^{1/2}$-level sensitivity for pseudomagnetic field measurements.

The aforementioned experiments are confined to scenarios where the alkali-metal and noble-gas spins are weakly coupled, specifically with $J/\beta \approx 6 \times 10^{-3}$. In this regime, the interaction strength between alkali-metal and noble-gas spins is significantly smaller than the decoherence rate of the alkali-metal spins. This weak interaction imposes constraints on quantum sensing, such as limiting the measurement bandwidth of our amplifier, i.e., $\widetilde{\Gamma}_b/2\pi \approx 5.7$ mHz. We further investigate how the performance of amplification evolves as the interaction strength increases and the two spin gases enter into the strong-coupling regime, unveiling previously unexplored amplification effects that are beneficial to precision measurements. In particular, we find that much broader amplification bandwidths are achievable with strong bidirectional interactions. To illustrate this, we discuss how the decoherence of noble gas changes as the interaction between alkali-metal and noble gases increases. When setting the detuning $\delta = 0$, the noble gas decoherence rate $\widetilde{\Gamma}_b$ is determined by (see Eq. **4**)

$$\widetilde{\Gamma}_b = \chi - \beta \mathbf{Im}[(J/\beta)^2 - 1]^{1/2}, \quad [5]$$

which directly determines the measurement bandwidth. By increasing the interaction J until reaching $J/\beta = 1$, the decoherence rate $\widetilde{\Gamma}_b$ can attain a maximum of $\widetilde{\Gamma}_b = \chi \approx \Gamma_a/2$ (*SI Appendix, Interacting spin gases*), allowing the measurement bandwidth to be half that of alkali-metal spins. Notably, further increasing J beyond $J/\beta = 1$ does not lead to additional improvements in the measurement bandwidth $\widetilde{\Gamma}_b$ because, when $J/\beta > 1$, $\mathbf{Im}[(J/\beta)^2 - 1]^{1/2} = 0$.

Unfortunately, achieving $J/\beta = 1$ remains unattainable in our ^{87}Rb to ^{129}Xe system because of the alkali-spin relaxation in collisions with xenon. As presented in the Appendix, we estimate the interaction strengths of existing pairs of alkali-metal and noble gases (*SI Appendix, Interaction strength of existing interacting atomic gases*). Our analysis indicates that one promising approach to achieving $J/\beta \geq 1$ is using the K-^{3}He system, which has a spin-destruction cross-section five orders of magnitude smaller than that of the ^{87}Rb to ^{129}Xe system. Consequently, the decoherence rate $\Gamma_a \approx 2\beta$ of K spins can be significantly reduced. In fact, $J/\beta \approx 10$ has already been successfully demonstrated in the K-^{3}He system (19). By further increasing the atomic number density of K and the pressure of ^{3}He (19, 38), it is anticipated that achieving $J/\beta > 100$ should be possible.

Although we have shown that increasing J/β beyond unity does not help to improve the bandwidth, we next show that it can enhance the magnetic amplification factor. According to *SI Appendix, Signal amplification*, the magnetic amplification in the strong-coupling regime $|q| \approx (\gamma_b \lambda M_z^b + \sqrt{J^2 - \beta^2})/\widetilde{\Gamma}_b$, indicating that improvements in bandwidth would inevitably deteriorate the amplification. Fortunately, entering the strong-coupling regime ($J/\beta > 1$) does not continue to increase $\widetilde{\Gamma}_b$, thereby preventing a reduction in q. Instead, we can focus solely on increasing J by raising the effective field λM_z^b of the

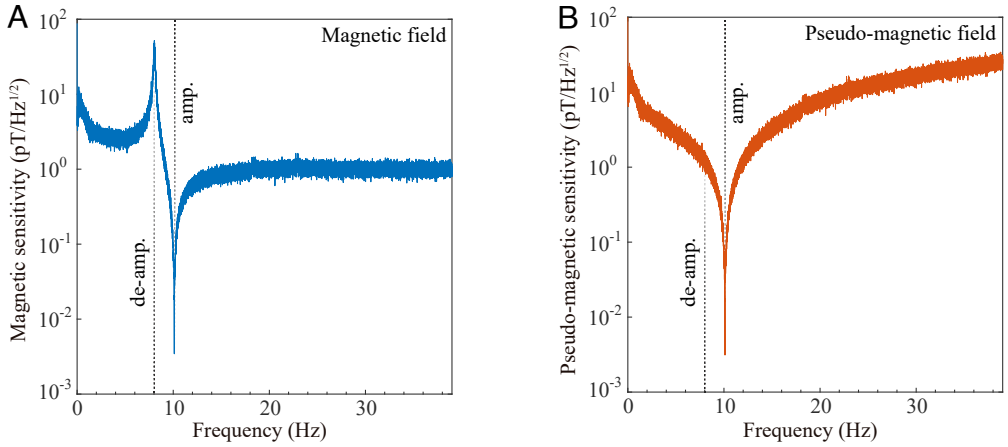

Fig. 4. Enhanced sensing assisted with amplification and deamplification. (*A* and *B*), the sensitivity to normal magnetic field and pseudomagnetic field (see text). The frequency of amplification and deamplification point is 10.11 Hz and 8.05 Hz, respectively. At the amplification point, the achieved normal magnetic-field sensitivity and the theoretical pseudomagnetic sensitivity is about 3.5 fT/Hz$^{1/2}$. At the deamplification point, the normal magnetic field is suppressed resulting in a deteriorated sensitivity, while the pseudomagnetic sensitivity is equal to the alkali-metal sensitivity that is about 1 pT/Hz$^{1/2}$.

noble gas to improve the amplification factor q. We estimate the potential amplification factor $|q|$ in strong-coupling regime. Specifically, we consider a K-^{3}He vapor cell with ^{3}He pressure exceeding 10 atm and spin polarization reaching up to 85% (38). When operating above 230 °C, the system is expected to reach $J/\beta \sim 100$ with $\lambda M_z^b \sim 100$ mG and $\widetilde{\Gamma}_b/2\pi \sim 5$ Hz. As a result, an amplification factor of $|q| \gtrsim 100$ is expected. Although the amplification in this regime is smaller than that in the weak coupling regime, it offers the unique advantage of realizing an atomic amplifier with both high bandwidth and a high amplification factor. Furthermore, when δ is zero, alkali metals experience a near-zero magnetic field, allowing operation within the spin-exchange relaxation-free (SERF) regime (22), potentially enabling their magnetic sensitivity to reach the sub-femtotesla per root hertz level. Combined with the aforementioned benefits, our results point to the potential for an unexplored type of quantum amplifiers with interacting spin gases. These amplifiers offer enhanced sensing amplification and bandwidth, with a potential sensitivity (including the amplification factor) on the order of 10 aT/Hz$^{1/2}$ under practical experimental conditions.

We would like to emphasize the main differences between our work and previous studies. Our work explores the bidirectional interaction between interacting alkali and noble atomic gases and reveals distinct amplification mechanisms absent in previous work, which assumed unidirectional interactions. This unidirectional interaction only considers the influence of noble gases on alkali metals, which simplifies the process of solving the coupled Bloch equations. Below, we highlight three key advancements enabled by bidirectional coupling. First, our work reveals that the Fano resonance effect originates from the bidirectional interaction and establishes a unified theory that encompasses both amplification and deamplification phenomena. In contrast, previous works (39–41) provided a phenomenological interpretation of the Fano profile and cannot predict key parameters like the Fano parameter and the deamplification point. Second, our work demonstrates the backaction of alkali metals on noble gases, which modifies the spin decoherence of noble gases and consequently influences the amplification mechanism. This effect remains significant even at weak interaction strengths, which is overlooked in earlier works (41–43) due to the unidirectional assumption. Third, our work extends the amplification mechanism to the strong-coupling regime, where the interaction strength exceeds the spin decoherence rates. Unlike previous works (42, 43), which were unable to address this regime, our work predicts several new effects. For example, we show there exists a significant enhancement in the frequency bandwidth of noble-gas amplification and provide a detailed discussion of the amplification mechanism under strong interaction regime. In addition, compared to traditional self-compensated comagnetometers (44, 45), which focus on the magnetic field response near the self-compensation point for near-DC fields, our work investigates the response under general bias magnetic fields B_z. Furthermore, we demonstrate that the self-compensation effect can be encompassed by the deamplification effect in our work (*SI Appendix, Comparison between deamplification and self-compensated effect*).

In summary, we demonstrate two distinct effects-amplification and deamplification-in interacting alkali-metal and noble-gas systems. Unlike previous magnetometers such as SERF (22), coherent population trapping (46), and nonlinear magneto optical rotation (47) magnetometers, which rely on the coherence within single-species atoms, the present approach leverages the interaction between different spin gases to work coherently, thus unlocking new potential for enhancing quantum sensing. Although our investigation focuses on the Rb-^{129}Xe system, our method is versatile and can be applied to a broad range of spin gas mixtures, including Rb-^{21}Ne and K-^{3}He. We further anticipate that enhancing atomic interactions to reach the strong-coupling regime will provide unprecedented means to efficiently control the properties of spin gases. Our initial findings validate this potential.

Data, Materials, and Software Availability. All study data are included in the article and/or *SI Appendix*.

ACKNOWLEDGMENTS. This work was supported by National Natural Science Foundation of China (Grant Nos. T2388102, 92476204, 12274395, and 12261160569, 124B2089, 123B2063), Innovation Program for Quantum Science and Technology (Grant No. 2021ZD0303205), Youth Innovation Promotion Association (Grant No. 2023474), and the XPLORER PRIZE. This work was also supported by the Cluster of Excellence "Precision Physics, Fundamental Interactions, and Structure of Matter" (PRISMA+ EXC 2118/1) funded by the German Research Foundation within the German Excellence Strategy (Project ID 39083149).

Author affiliations: [a]Laboratory of Spin Magnetic Resonance, School of Physical Sciences, University of Science and Technology of China, Hefei 230026, China; [b]Anhui Province Key Laboratory of Scientific Instrument Development and Application, University of Science and Technology of China, Hefei 230026, China; [c]Hefei National Laboratory, University of Science and Technology of China, Hefei 230088, China; [d]Helmholtz Institute Mainz, Mainz 55099, Germany; [e]GSI Helmholtzzentrum für Schwerionenforschung GmbH, Darmstadt 64291, Germany; [f]Institute for Physics, Johannes Gutenberg University, Mainz 55128, Germany; and [g]Department of Physics, University of California, Berkeley, CA 94720-7300

1. J. P. Gordon, H. J. Zeiger, C. H. Townes, Molecular microwave oscillator and new hyperfine structure in the microwave spectrum of NH_3. *Phys. Rev.* **95**, 282 (1954).
2. N. Basov, A. Prokhorov, Theory of the molecular generator and molecular power amplifier. *Sov. Phys. JETP* **3**, 426 (1956).
3. A. A. Clerk, M. H. Devoret, S. M. Girvin, F. Marquardt, R. J. Schoelkopf, Introduction to quantum noise, measurement, and amplification. *Rev. Mod. Phys.* **82**, 1155 (2010).
4. P. G. O'Shea, H. P. Freund, Free-electron lasers: Status and applications. *Science* **292**, 1853 (2001).
5. J. P. Gordon, H. J. Zeiger, C. H. Townes, The maser-new type of microwave amplifier, frequency standard, and spectrometer. *Phys. Rev.* **99**, 1264 (1955).
6. T. Maiman, Stimulated emission of radiation in ruby. *Nature* **187**, 493 (1960).
7. L. Jin *et al.*, Proposal for a room-temperature diamond maser. *Nat. Commun.* **6**, 1–8 (2015).
8. J. D. Breeze, E. Salvadori, J. Sathian, N. M. Alford, C. W. Kay, Continuous-wave room-temperature diamond maser. *Nature* **555**, 493–496 (2018).
9. M. Oxborrow, J. D. Breeze, N. M. Alford, Room-temperature solid-state maser. *Nature* **488**, 353–356 (2012).
10. H. Wu *et al.*, Enhanced quantum sensing with room-temperature solid-state masers. *Sci. Adv.* **8**, ade1613 (2022).
11. A. L. Schawlow, C. H. Townes, Infrared and optical masers. *Phys. Rev.* **112**, 1940 (1958).
12. T. G. Walker, W. Happer, Spin-exchange optical pumping of noble-gas nuclei. *Rev. Mod. Phys.* **69**, 629 (1997).
13. M. Balser, C. A. Wagner, Observations of earth-ionosphere cavity resonances. *Nature* **188**, 638–641 (1960).
14. M. Jiang, H. Su, A. Garcon, X. Peng, D. Budker, Search for axion-like dark matter with spin-based amplifiers. *Nat. Phys.* **17**, 1402–1407 (2021).
15. S. Afach *et al.*, Search for topological defect dark matter with a global network of optical magnetometers. *Nat. Phys.* **17**, 1396–1401 (2021).
16. A. Arvanitaki, A. A. Geraci, Resonantly detecting axion-mediated forces with nuclear magnetic resonance. *Phys. Rev. Lett.* **113**, 161801 (2014).
17. I. M. Bloch *et al.*, New constraints on axion-like dark matter using a floquet quantum detector. *Sci. Adv.* **8**, eabl8919 (2022).
18. O. Katz, R. Shaham, O. Firstenberg, Quantum interface for noble-gas spins based on spin-exchange collisions. *PRX Quantum* **3**, 010305 (2022).
19. R. Shaham, O. Katz, O. Firstenberg, Strong coupling of alkali-metal spins to noble-gas spins with an hour-long coherence time. *Nat. Phys.* **18**, 506–510 (2022).
20. T. R. Gentile, P. Nacher, B. Saam, T. Walker, Optically polarized ^{3}He. *Rev. Mod. Phys.* **89**, 045004 (2017).
21. E. Ressayre, A. Tallet, Holstein-primakoff transformation for the study of cooperative emission of radiation. *Phys. Rev. A* **11**, 981 (1975).
22. I. Kominis, T. Kornack, J. Allred, M. V. Romalis, A subfemtotesla multichannel atomic magnetometer. *Nature* **422**, 596–599 (2003).
23. D. Budker, M. Romalis, Optical magnetometry. *Nat. Phys.* **3**, 227–234 (2007).

24. M. Bulatowicz *et al*., Laboratory search for a long-range t-odd, p-odd interaction from axionlike particles using dual-species nuclear magnetic resonance with polarized ^{129}Xe and ^{131}Xe Gas. *Phys. Rev. Lett.* **111**, 102001 (2013).
25. S. B. Zhang *et al*., Search for spin-dependent gravitational interactions at earth range. *Phys. Rev. Lett.* **130**, 201401 (2023).
26. T. G. Walker, M. S. Larsen, Spin-exchange-pumped NMR gyros in Advances in atomic, molecular, and optical physics. *Elsevier* **65**, 373–401 (2016).
27. S. L. Bernstein *et al*., Long-range communications at extremely low frequencies. *Proc. IEEE Inst. Electr. Electron. Eng.* **62**, 292–312 (1974).
28. A. Fraser-Smith, J. Buxton, Superconducting magnetometer measurements of geo-magnetic activity in the 0.1-to 14-hz frequency range. *J. Geophys. Res.* **80**, 3141–3147 (1975).
29. J. Kawai *et al*., Characterization and demonstration results of a squid magnetometer system developed for geomagnetic field measurements. *Supercond. Sci. Technol.* **30**, 084002 (2017).
30. J. Preskill, M. B. Wise, F. Wilczek, Cosmology of the invisible axion. *Phys. Lett. B* **120**, 127–132 (1983).
31. L. F. Abbott, P. Sikivie, A cosmological bound on the invisible axion. *Phys. Lett. B* **120**, 133–136 (1983).
32. M. Dine, W. Fischler, The not-so-harmless axion. *Phys. Lett. B* **120**, 137–141 (1983).
33. D. Budker, P. W. Graham, M. Ledbetter, S. Rajendran, A. O. Sushkov, Proposal for a cosmic axion spin precession experiment (CASPEr). *Phys. Rev. X* **4**, 021030 (2014).
34. C. Abel *et al*., Search for axionlike dark matter through nuclear spin precession in electric and magnetic fields. *Phys. Rev. X* **7**, 041034 (2017).
35. B. A. Dobrescu, Mocioiu I (2006) Spin-dependent macroscopic forces from new particle exchange. *J. High Energy Phys.* **11**, 005 (2006).
36. M. Vysotsskii, Y. B. Zel'Dovich, M. Y. Khlopov, V. Chechetkin, Some astrophysical limitations on the axion mass. *JETP Lett.* **27**, 533 (1978).
37. G. G. Raffelt, Astrophysical axion bounds in Axions. *Springer* **741**, 51–71 (2008).
38. W. Chen, T. Gentile, Q. Ye, T. Walker, E. Babcock, On the limits of spin-exchange optical pumping of ^{3}He. *J. Appl. Phys.* **116**, 014903 (2014).
39. M. Jiang *et al*., Observation of magnetic amplification using dark spins. *Proc. Natl. Acad. Sci. U.S.A.* **121**, e2315696121 (2024).
40. M. Xu *et al*., Cooperative spin amplifier for enhanced quantum sensing. *Phys. Rev. Lett.* **133**, 133202 (2024).
41. H. Su, M. Jiang, X. Peng, Review of noble-gas spin amplification via the spin-exchange collisions. *Sci. China Inf. Sci.* **65**, 200501 (2022).
42. M. Jiang *et al*., Floquet spin amplification. *Phys. Rev. Lett.* **128**, 233201 (2022).
43. Y. Qin *et al*., New classes of magnetic noise self-compensation effects in atomic comagnetometer. *Phys. Rev. Lett.* **133**, 023202 (2024).
44. T. Kornack, M. Romalis, Dynamics of two overlapping spin ensembles interacting by spin exchange. *Phys. Rev. Lett.* **89**, 253002 (2002).
45. T. Kornack, R. Ghosh, M. Romalis, Nuclear spin gyroscope based on an atomic comagnetometer. *Phys. Rev. Lett.* **95**, 230801 (2005).
46. V. Shah, S. Knappe, P. D. Schwindt, J. Kitching, Subpicotesla atomic magnetometry with a microfabricated vapour cell. *Nat. Photonics* **1**, 649–652 (2007).
47. D. Budker *et al*., Resonant nonlinear magneto-optical effects in atoms. *Rev. Mod. Phys.* **74**, 1153 (2002).